Ultralight Ladder-type Coilable Space Structures

Fabien Royer* and Sergio Pellegrino†

California Institute of Technology,1200 E California Blvd.,Pasadena, CA 91125

We describe the concept of an ultralight ladder-type coilable strip used as the main element to build large planar deployable space solar power spacecrafts. It is composed of TRAC longerons connected with lenticular cross-section rods which enables it to fully flatten and thus be packaged efficiently. The design is tackled here as well as the manufacturing of a scaled version of this new type of structures. Finite element analyses are used to understand the underlying behavior of such structures. Experimental modal testing is then used as a way of validating this computational framework. Finally a simulation framework enabling simulation at the spacecraft scale is presented and preliminary results obtained with shows how such structures behave while integrated into a larger spacecraft.

I. Introduction

We are currently investigating structural architectures for ultralight, coilable space structures suitable for large, deployable, flat spacecraft supporting large numbers of identical tiles that act both as collectors of photovoltaic (PV) energy and radio frequency (RF) radiators. We envisage large constellations of such spacecrafts, collecting solar power in space and beaming it to Earth. The PV part of the tile contains a series of parabolic reflectors that focus the incoming light onto thin PV strips mounted on the back of the reflectors.[1] The current is converted into microwave radiation in the RF part of the tile, and a common time reference between all tiles allows the formation of a phased array of rectifying antennas, enabling beam-forming and beam-steering.[2]

The concept that is being pursued by the Space-based Solar Power Initiative (SSPI) at Caltech is schematically shown in Figure 1. In the deployed configuration, each spacecraft is 60 m $\times$ 60 m in size and is composed of ultralight ladder-type coilable strips of equal width, arranged to form a square, and each strip supports many tiles. The whole structure is folded and packaged using a folding pattern derived from origami techniques by coiling the strips as explained in a previous paper.[3]

A review of previously proposed structural concepts[3] showed several approaches based on kilometer-scale structures that would require in-orbit robotic assembly as well as some modular solutions that could be implemented through deployable membrane-like structures. The concept proposed herein resembles more closely advanced solar-array architectures such as the Roll-Out Solar Array (ROSA)[5] and the the Roll-Out and Passively Deployed Array (RAPDAR).[6] These structures make use of coilable booms to deploy and tension a flexible array of photovoltaic cells.

A key element of our proposed structures is the coilable strip, for which a ladder-like architecture has been proposed, and this architecture is described in more detail in the next section. This paper addresses key aspects of the strip design, through prototyping, analysis and experimental model validation. It is composed of two collapsible TRAC longerons connected transversally by rod like structures called battens. A specific design for the battens is proposed, as well as a scheme for integrating battens and longerons. A prototype of the strip is built to assess manufacturability of the proposed solution and to validate experimentally the finite element model (FEM) we developed. Finally, this FEM is integrated into a larger model that simulates the SSPI module using a parametric framework. Preliminary results on the module modal analysis are shown for a 2 m module and extension to larger scales are discussed in the conclusion section.

*Graduate Student, Graduate Aerospace Laboratories at the California Institute of Technology (GALCIT), 1200 E California Blvd. MC 205-45

†Joyce and Kent Kresa Professor of Aeronautics and Professor of Civil Engineering, Graduate Aerospace Laboratories, California Institute of Technology (GALCIT), 1200 E California Blvd. MC 105-05. AIAA Fellow

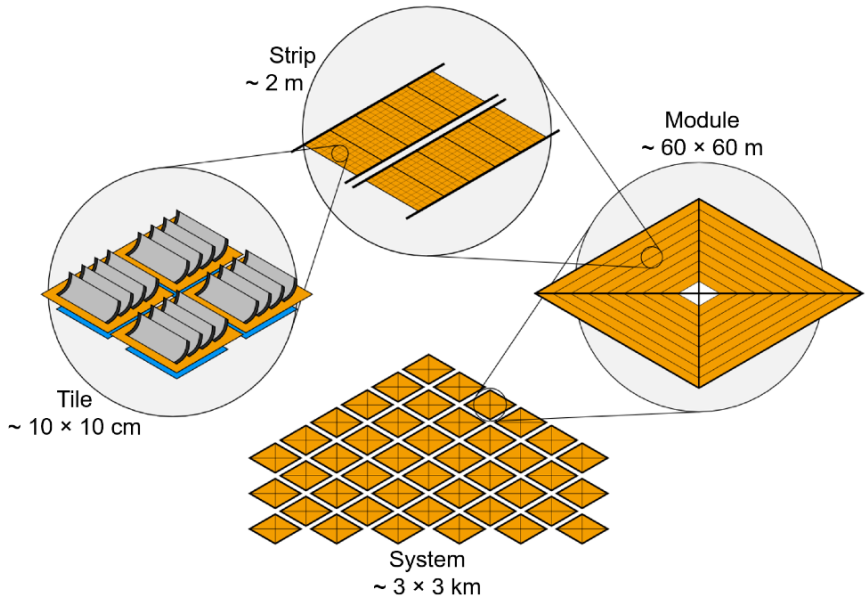

Figure 1. Overview of Space-based Solar Power Initiative concept pursued at Caltech.

II. Strip Design

II.A. Battens and Longerons

The general concept for the strip structure is shown in figure 2. It consists of two triangular rollable and collapsible (TRAC)[4] longerons, connected transversely by rod-like structures (battens) which support the tiles. The strip is assumed to carry static loads primarily in bending and the required bending stiffness can be obtained by imposing the constraint that the maximum slope of the tiles during operation, i.e. under solar pressure loading (9 µPa), should not exceed 1 deg in order to maintain near-optimal performance of the solar concentrators. Thus, it has been shown[3] that an adequate design for the longerons uses the cross-section sketched in figure 2.

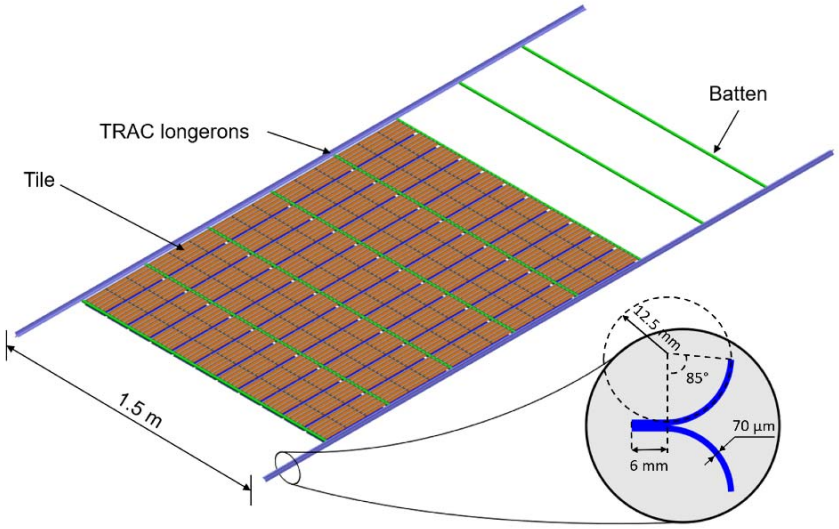

Figure 2. Detail of strip composed of tiles, battens and TRAC longerons.[3]

The functional tiles supported by the strips are able to flatten. In order to achieve a high packaging efficiency, the strip also has to flatten completely, which requires the battens to be collapsible. The chosen architecture consists of rods with lenticular cross-section. The batten cross-section has been derived from a standard lenticular shape with added flat sections at the top and bottom, for ease of bonding the tiles, see Figure 3. The battens are made of a composite material and two different layups have been studied: a [0,90] layup of carbon fiber reinforced plastic as well as a [0,90] glass fiber plain weave. The radius of the two semi-circles of the cross-section has been chosen according to the three following requirements.

1. Its value has to be greater than the one for which the maximum strain when the cross-section is flattened reaches the limit strain of the material. This prevents failure of the battens due to coiling of the strip.

2. The module is divided into 4 quadrants, and each quadrant corresponds to a 45°angular sector. It yields that the end of the strips are cut at 45°which makes the length of the inner longeron and outer longeron different. As a result, the static bending deformations as well as natural bending modes are coupled with the torsion deformation of the strip (described in section II.C). Simulations of an element of strip have been carried out (not detailed in this paper) and showed that there exists a minimum second moment of area for the batten cross-section, under which the battens start buckling as the strip twists which reduces dramatically the strip torsional stiffness. The chosen radius ensures that the battens are not buckling for the initial range of twist consider (maximum twist of 5 deg).

3. Finally we must limit the mass of the structures to cope with launch constraints. It yields that the radius should be as small as possible without violating the two previous requirements, in order to limit the amount of material used to make the batten.

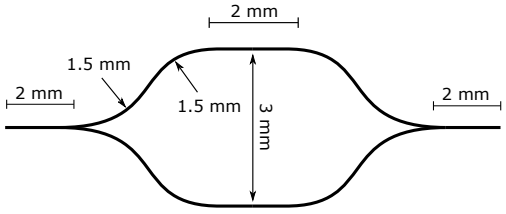

Figure 3. Detail of lenticular cross-section with flat top and bottom used in the strip, with its relevant dimensions.

II.B. Connection Batten/Longeron

In order to be able to coil the strip, the connection used between the batten and the longeron has to be collapsible as well. The current design of the connection between batten and longeron is shown in Figure 4. The cross-section is closed at the connection, to maximize the torsional stiffness of the batten, and thus the torsional stiffness of the strip. The batten is pinched flat at both ends and embedded within the TRAC longerons. It creates a transition region of length approximately equal to 15 mm.

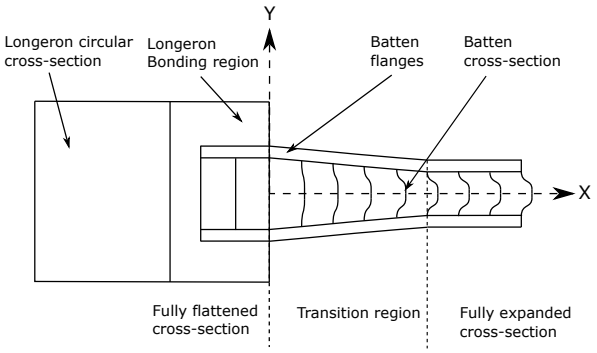

Figure 4. Scheme used to connect longerons and battens. The end of the batten is flattened and embedded into the TRAC longeron bonding region. This creates a transition region where the cross-section goes from fully flatten to fully expanded.

III. Strip Finite Element Analysis

III.A. Finite Element Model

Simulations of high fidelity strip models have been performed using ABAQUS Standard. We studied strips of length ranging from 10 m to 60 m, in order to study their behavior across the scales. In this model, the longerons are made of a 4 plies [0,90]s layup of carbon fiber reinforced plastic. The battens are of the same material but are only made of 2 plies [0,90] and both longerons and battens are meshed using S4R shell elements. The lenticular batten geometry is generated in its undeformed state. A prior simulation flattens both ends on a length of 4 mm and the deformed geometry is then imported into the strip model and tied on the longeron as shown in figure 5. The strip is simply supported at the end cross-sections of the inner and outer longerons. A frequency analysis was carried out and the 30 first natural frequencies of each model were extracted.

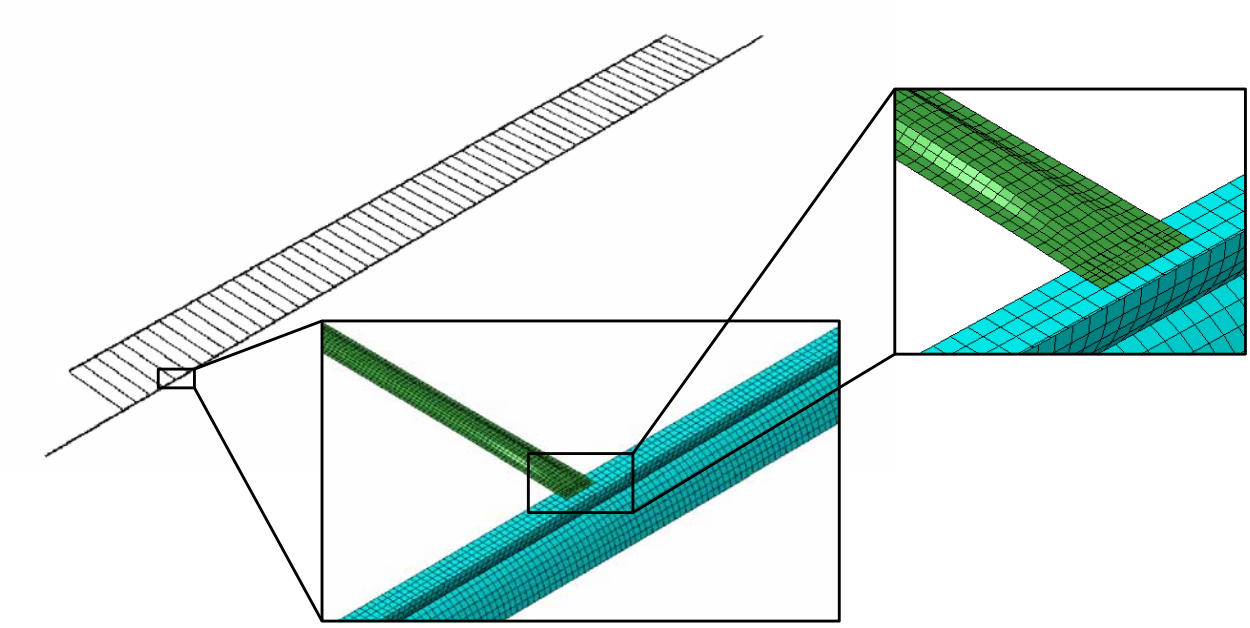

Figure 5. Finite element model of a 20 m strip. Detail of the flattened end of a batten being attached to the longeron is shown.

III.B. Results

The 10 first mode shapes for the 50 m strip are presented in figure 6. The first observation that can be made is that the frequencies are relatively low. This is not a surprise since we are dealing with large structures. We distinguish out-of-plane bending modes, torsion modes as well as in-plane modes. However the strip is made such that its end is cut at 45°, in order to be assembled into quadrant as mention before. As a result, the inner longer and outer longeron have a different length and vibrates at their own frequencies, like two independent beams in bending. The comparison between the obtained natural frequencies and the theoretical natural frequencies of an equivalent beam with half of the strip mass, longeron second moment of area and homogenized material properties is highlighted in table 1. The length is taken to be the average between the inner and outer longeron lengths. The beam model seems to be capturing the first bending mode perfectly and becomes less accurate for higher order modes even though it is still a good first order approximation. This quasi-independent vibration of both longerons creates a coupling between out-of-plane bending, and twisting of the strip as seen on mode 1, 5, 8 and 10. In addition the length mismatch between inner and outer longeron results in a different sinusoidal vibration amplitude for each longeron and thus a different slope at the batten/longeron connection at each end. This results in torsion being applied on the battens. Since the differential of angle is more pronounced for higher order bending modes, it could explain the discrepancy between the theoretical beam model and the extracted frequencies above mode 1, as the battens torsion participation into the overall strip "bending" stiffness becomes non-negligible. The battens are also subject to torsion when the strip experience twisting.

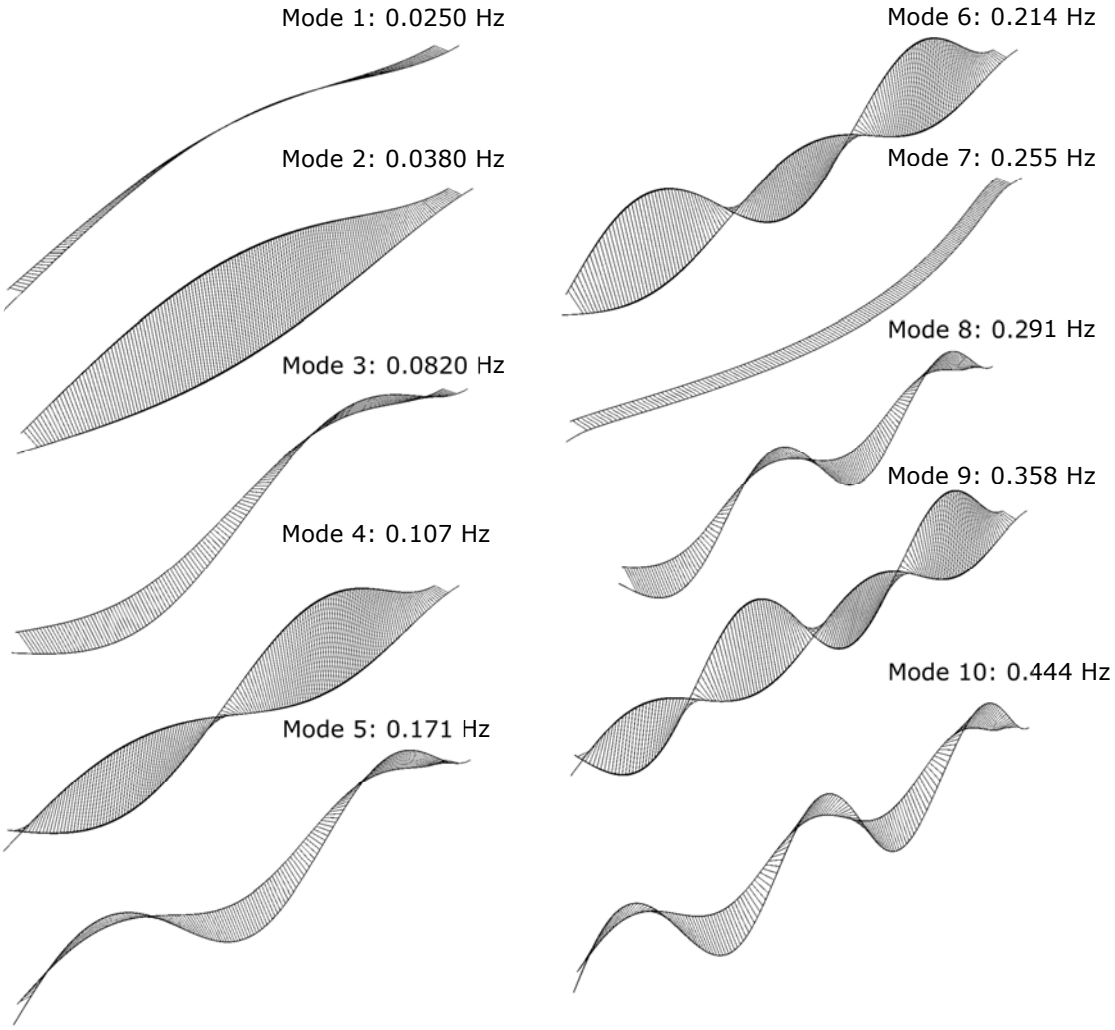

Figure 6. 10 first modes of a 50 m strip extracted from finite element simulations.

Strip Mode Number	FEM frequency (Hz)	Theoretical Beam Frequency (Hz)	Relative Error (%)
1	0.012	0.012	0
3	0.045	0.049	8.9
5	0.10	0.11	10
7	0.18	0.197	9.4
10	0.28	0.307	9.6

Table 1. Comparison of out-of-plane bending frequencies extracted from the FEM of a 50 m strip to the theoretical bending frequencies of a beam with homogenized properties.

Next, consider the influence of the strip length on the vibration frequencies, plotted against the strip length in figure 7. The frequency decreases in a parabolic fashion which was to be expected since the theoretical vibration frequency of a beam in bending is inversely proportional to the square of its length, and we show that the beam model is a relatively good first order approximation. We can further that the order of the modes switches at certain strip length. This is not surprising and occurs between modes of different nature (out-of-plane bending, torsion, in-plane bending). Another interesting way of seeing the scale effect on frequencies is to plot these as a function of the mode number for the considered range of length, and is shown in figure 8. The mode frequency grows almost linearly for strip lengths under 20 m. However, for the 20 m strip and 10 m strip, the linear trend stops and is followed by a plateau (in fact a linear trend with very small slope). This marks the limit between the longeron dominated vibration modes and the batten dominated vibration modes. When the frequency is high enough to reach the first vibration frequency of the battens, energy is taken from the longeron modes and redistributed to the batten modes, which reduces the effective modal mass associated to the longeron deformation.

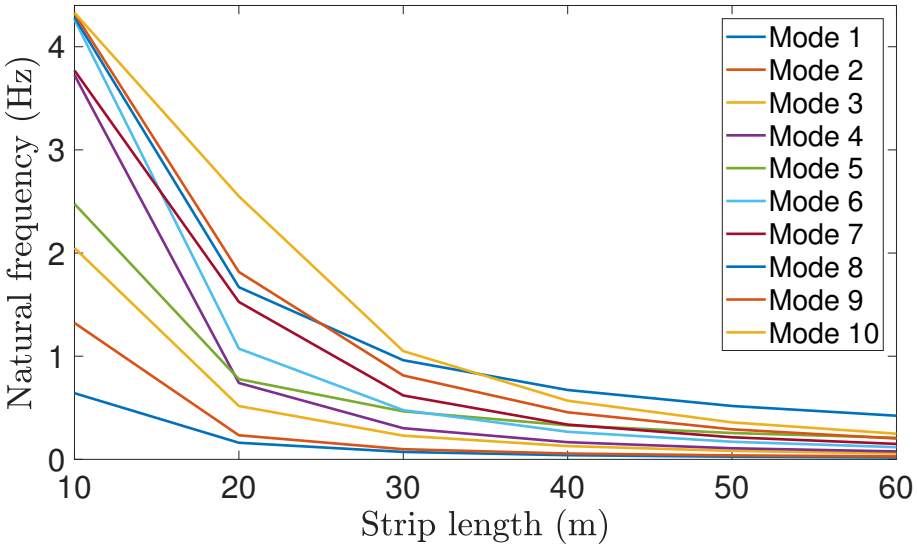

Figure 7. Evolution of strip natural frequencies as function of its length, for the ten first vibration modes.

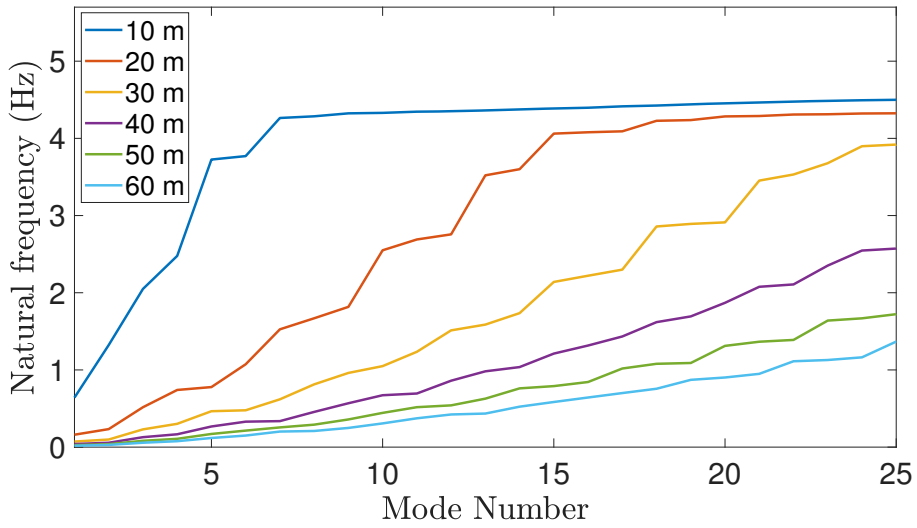

Figure 8. Evolution of strip natural frequencies as function of the mode number, for the studied range of strip lengths.

Finally, since we saw that the battens are undergoing torsion in almost every vibration modes, we wish to understand how they behave when twisted particularly in the transition region that arise from the batten/longeron connection. Therefore a last analysis at the strip level has been undertaken. A twist of 1.5 deg is applied in the middle of a 10 m strip and the local rotation along the batten axis of the nodes located inside the batten transition region have been extracted. The result is plotted in figure 9. The coordinates X and Y corresponds to the location of the considered node inside the transition region as sketched earlier in figure4. One can observe that the side of the battens ($Y > 2$) is twisting a lot while the rotation of the center part remains relatively less significant. The longeron prescribed angle propagates through the flanges that have a much smaller second moment of area than the central cross-section. The batten torsional stiffness in that region then becomes highly non-uniform due to this differential twist . Outside the transition region, the batten shows almost no twist. Therefore, the compliant flanges at the connection act like torsion "isolators". This is rather interesting for our application since the functional tiles are fixed on the battens, and torsion across the full length of could potentially be an issue.

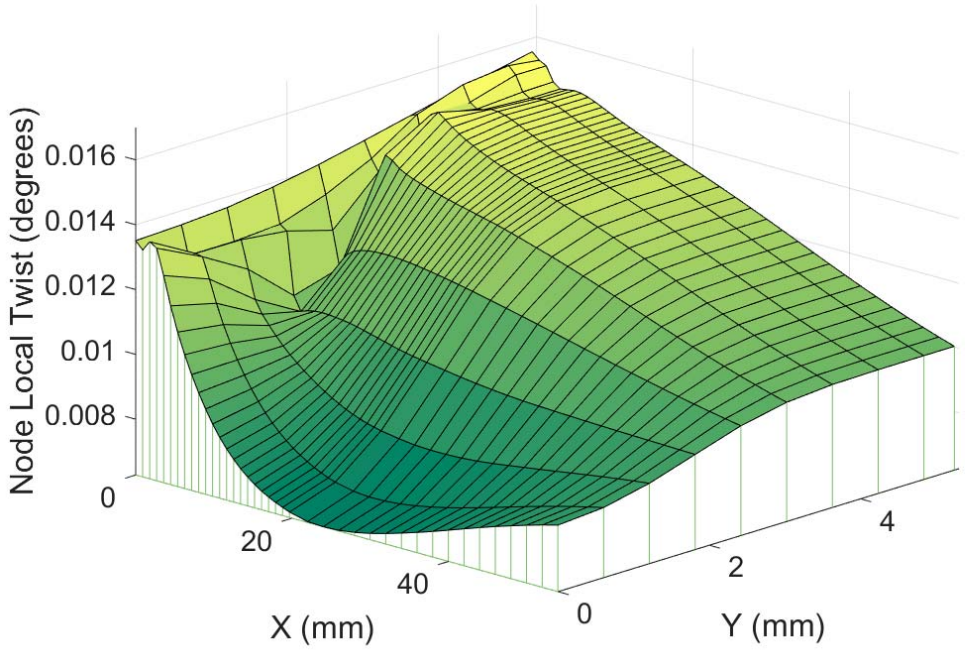

Figure 9. Local twist of the transition region nodes. The coordinates X and Y refers to the position in the transition region and is described in figure4.

IV. Physical Prototype and Model Validation

IV.A. Components Manufacturing

The TRAC longerons manufacturing process has been developed and characterized by Christophe Leclerc.[7] They are made of [0,90]s layup of 17 gram per square meter (gsm) uni-directional tape supplied by North Thin Ply Technology (fibers T800 and epoxy resin ThinPreg 120EPHTg-402). An additional step is added to the process and consists in placing 20 mm wide Teflon strips in the TRAC longeron bonding region. This creates local 20 mm gaps which enables the battens to be slid and embedded into the longeron.

For the battens, the use of various materials have been investigated. The first approach consists in manufacturing the battens with the same material as the longerons. The cured thickness per ply is around 17 µm. The layup is composed of two plies, [0,90]. However, those components were relatively difficult to handle due to the high curvatures of the cross-section that yields high stresses. For the thickness considered, the material is very sensitive to imperfections which lead to the formation of cracks. As an alternative, a 31 gsm glass fiber preimpregnated plain weave has been used to build more robust battens for the sack of prototyping and testing a representative element of strip for a 2 m scale version of the module. Two plies

are stacked together to create a [0,90] layup. The cured thickness per ply is around 80 µm. A manufacturing process has been developed to perform fast prototyping of battens in one cure, using a combination of male and female silicone rubber molds constrained in aluminum cages and obtained using 3D printed parts. Those molds are shown in Figure 10. The process uses the difference in thermal expansion between silicone rubber and aluminum, as well as the silicone rubber quasi-incompressibility to apply high pressure on the layup without changing the cross-section shape. The battens produced are about 500 mm long which will then be extended to longer ones in the future. Pictures of lenticular battens obtained with this process are shown in figure 11. The battens and the longerons are then assembled using the connection method described in section II.B.

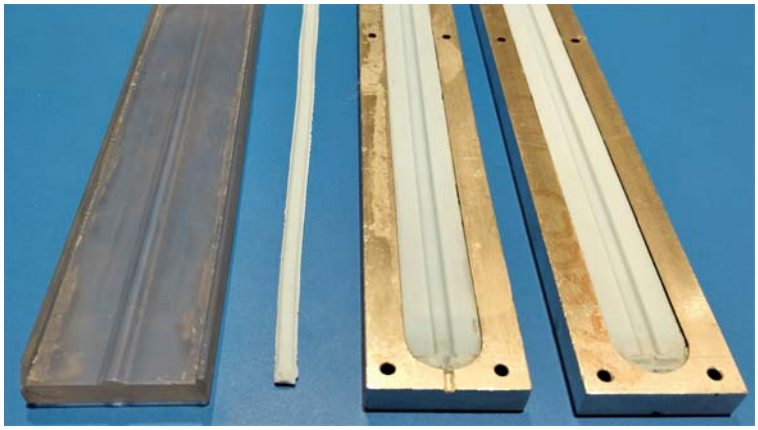

Figure 10. Silicone rubber molds used to manufacture the lenticular battens. The 3D printed part shown on the left is used to mold the blue female silicone plugs enclosed in their aluminum cages. The male silicone plug is directly molded from the female silicone plugs.

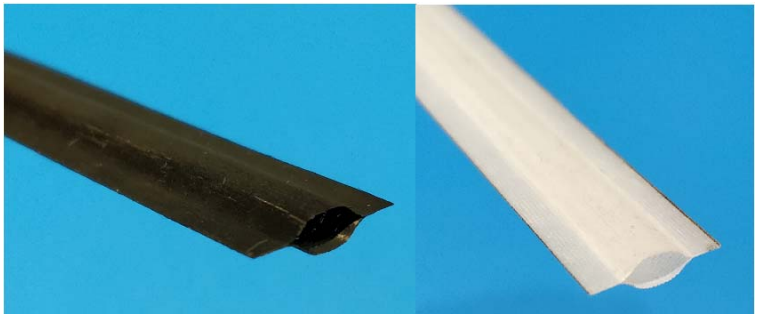

Figure 11. Carbon fiber batten is shown on the left and glass fiber batten is shown on the right.

IV.B. Small Scale Strip Assembly

In order to verify the robustness of the connection scheme between the TRAC longerons and the battens, a representative element of strip has been assembled. It corresponds to the dimensions of a 2 m scale module (20 cm long battens, with 20 cm spacing between them). Three battens are manufactured using the process described above as well as two 54 cm long longerons. The final strip prototype weights 7.36 g. The result is shown in figure 12.

IV.C. Experimental validation

In order to validate the modeling of the strip and particularly to assess our ability to correctly capture the thin shell behavior, a modal test of the strip prototype is conducted. The test setup is presented in figure 13. The strip is suspended on soft springs attached to an aluminum rig and is excited transversely by a stinger mounted on a shaker. We run a sine sweep ranging from 0 Hz to 10 Hz. Reflective targets are placed at various locations on the strip and we use a scanning laser vibrometer to extract the motion of those targets during the sweep, in order to reconstruct the strip frequency response function. The natural modes of the

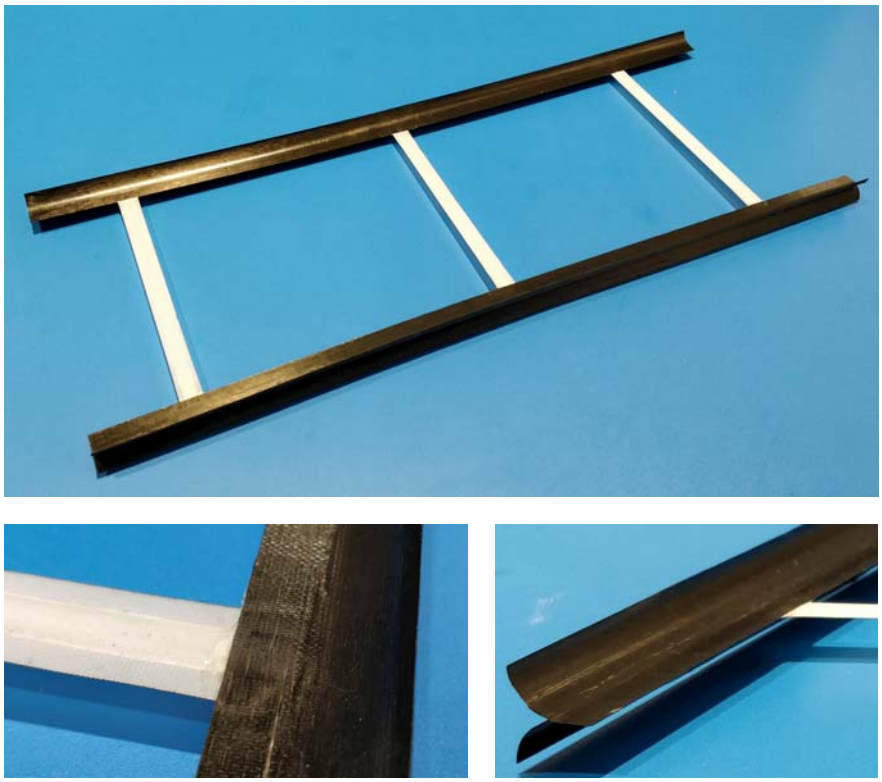

Figure 12. 54 cm long strip prototype. Detail of the connection between batten and longeron is shown as well as the longeron cross-section.

structure are extracted and compared to a FEM of the strip prototype, also shown in figure 13. This FEM is generated using the same process as described in section II.A. In the range of interest, the first two modes are rigid body motions and the first deformation mode is the first torsion mode of the strip. There is no other deformation mode in this range, and we thus focus on the first torsion mode for our analysis.

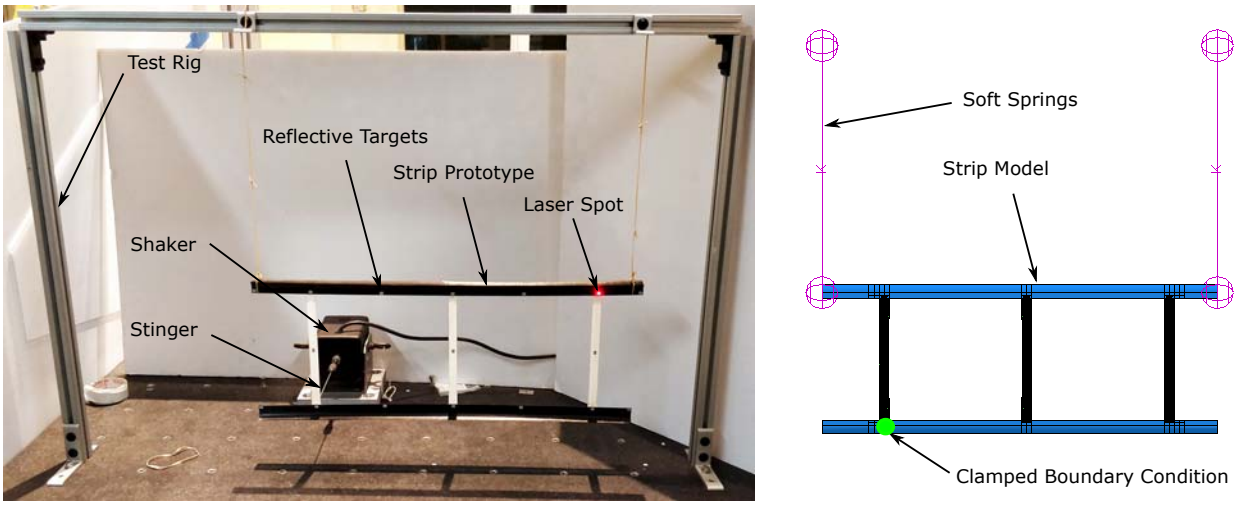

Figure 13. Model validation experiment is presented on the left and compared to the finite element model shown on the right, that aims at reproducing accurately the experiment.

The first torsion mode extracted from the FEM and the one obtained by reconstruction from the scanning laser vibrometer data look qualitatively the same and are shown in figure14. However the predicted mode frequency extracted from the simulation gives 5.64 Hz whereas the experimentally obtained frequency amounts to 6.88 Hz, although the rigid body modes frequencies are matching. This implies that the tor-

sional stiffness of the strip prototype is higher than the FEM one. As mentioned earlier, the role of the torsional stiffness of the batten/longeron connection in the strip torsional stiffness is predominant. Looking more closely at the prototype, it is noticeable that while bonding the battens into the longerons, an excess of epoxy has been applied. It results in epoxy flowing and filling the cross-section on a length of several millimeters in the transition region, making it quasi-rigid. This is shown in figure 15. To simulate this effect, rigid body constraints have been applied to the transition region elements on a length of 6 mm (this value changes for every connection in the prototype, this is an average). The frequency obtained with this updated FEM gives 6.67 Hz which reduces dramatically the discrepancy. The remaining error is due to the fact that the epoxy distribution is varying for every connection. This mismatch can easily be fixed in future prototype by monitoring more thoroughly the amount of epoxy applied at the connections. Two conclusions can be drawn from this comparison. The first one is that the model, after correction seems to perform correctly and the main discrepancy seems to come from prototyping considerations. The second one is that we have the confirmation here that the transition region torsional stiffness plays a key role in the strip torsional stiffness. As a result one can not capture accurately the torsional stiffness of a strip by considering homogenized model such as an equivalent plate. The connection behavior has to be fully resolved in FEM of the strip and the module tackled in the next section.

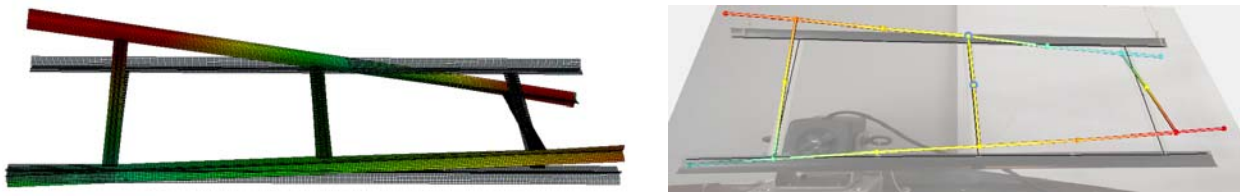

Figure 14. First torsion mode obtained from the FEM is shown on the left, and look similar to the experimental mode extracted from the laser vibrometer data, shown on the right.

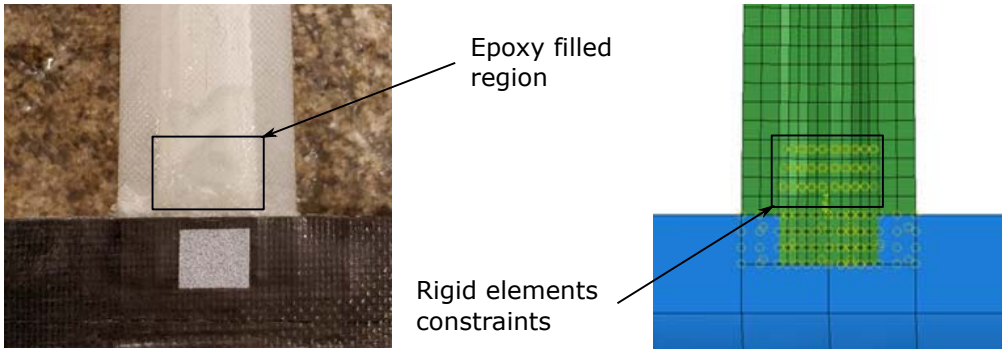

Figure 15. Detail of connection transition region on the prototype (on the left) compared to the FEM model of the same connection. The epoxy filled region is modeled with rigid elements.

V. Module Structure Simulation

V.A. 2 m Module Finite Element Model

A high fidelity finite element model of the structure is required to assist the design process. It enables conducting trade-off analyses at the system level, rapidly assess the impact of specific architecture design choices as well as getting more insights into the interactions between components and the effect of boundary conditions on the system's mechanical response. This simulation is particularly suitable to assess the static and dynamic performance of the spacecraft structure and open the door to broader type of analyses such as multiphysics studies. In order to achieve the goals mentioned above, the finite element model has to be highly modular, parametric and computationally effective. The specificity of this architecture is that it is highly hierarchical and is described using two main length scales. One is related to the cross-section of the battens and the TRAC longerons and is in the order of several millimeters. A fine mesh need to be used to describe the non-linear behavior at the connection between those components. However, the length of the

longerons (i.e. the length of the strip) can reach up to 60 m which requires a coarser mesh in order to be computationally tractable. Therefore the use of model reduction procedures appears to be relevant and will be discussed at the end of this section. The bulk of the analysis as so far been performed on a 2 m scale module. Even though this size seems far from the 60 m module envisioned in the long term, it allows the manufacturing and testing of prototypes in the laboratory as well as flight prototypes suitable for CubeSat type missions. The code written to generate the FEM is highly parametric and therefore can also generate modules of other sizes and geometry. The model is described in figure 16.

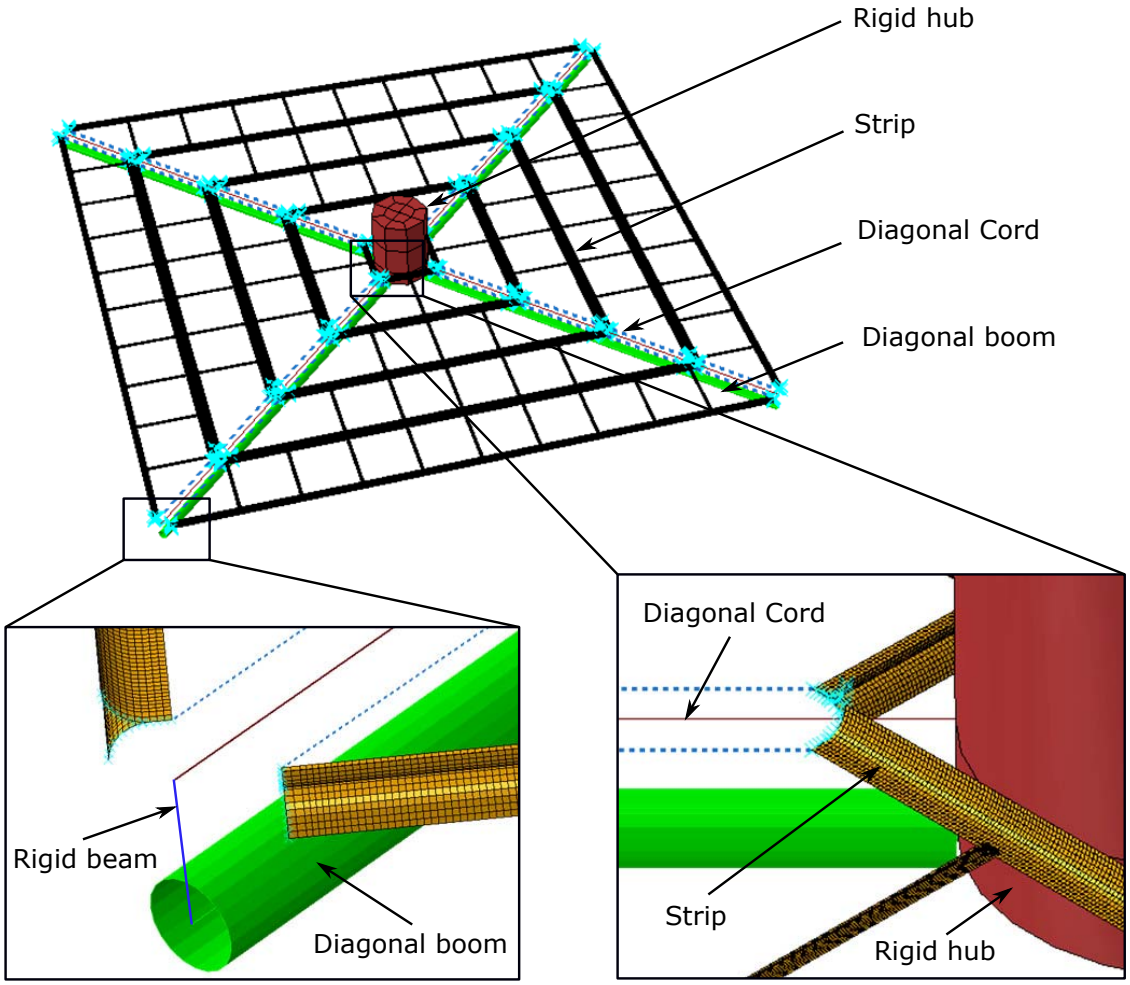

Figure 16. Finite element model of the SSPI spacecraft structure.

The side length of the module is 2 m and the module is composed of 4 strips per quadrant. On each of the strips, the battens spacing is 20 cm and the batten length is 20 cm as well. In this first attempt, the tiles geometry and stiffness where not included in the model, but their mass is added uniformly to the battens. Since we wish not to stress the tiles (to prevent any concentrators shape change) during module deformation, this latest assumption seems to be reasonable and captures this requirement. However further work on the attachment between the tiles and the module will be carried out to verify or mitigate the tiles influence on the module stiffness. A axial prestress is applied to the cords by the diagonal booms. Finally each strip is mounted in a kinematic way on the diagonal cords. The inner longeron is attached to the cord using a revolute joint on one side, and the longeron out-of-plane displacement is tied to the cord out-of-plane displacement on the other side. The outer longeron is attached in a similar fashion, but the role of the two sides are permuted. This scheme allows to prestress the cords uniformly without prestressing the strips. The attachment scheme is sketched in figure 17.

The spacecraft structure is composed of a rigid cylinder called hub which models the spacecraft bus. Four diagonal booms deploy from the hub. In reality those would be coilable booms but for the purpose of this analysis, we consider that those booms are tubular beams with radius 15 mm and thickness 0.2 mm

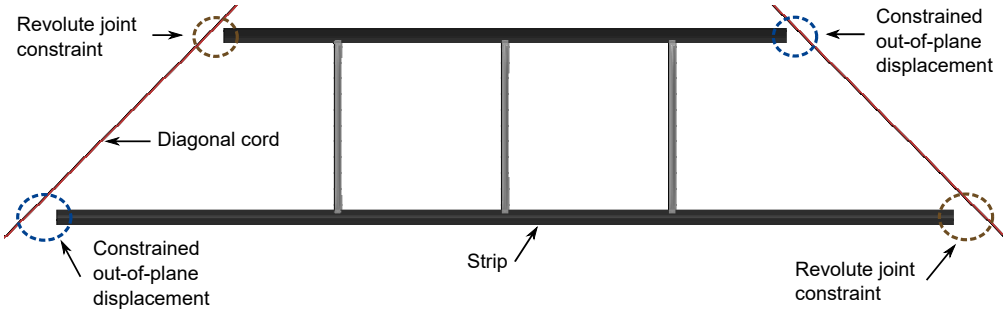

Figure 17. The strips are mounted in a kinematic way on the diagonal cords which enables prestressing the cords without prestressing the strips.

made of glass fiber. They support and tension four diagonal cords that are attached via a rigid beam to the booms and pined on the other end on the hub. The later is held fixed and a prestress of 1 N is applied to each of the 4 cords. The 30 first vibration frequencies and mode shapes of the system are computed. The first qualitative observation is that the frequencies are relatively low, which is what was expected for this relatively flexible structures. The 30 first natural frequencies extend from 0.13 Hz to 2.37 Hz. For the bottom of this spectrum (below 1 Hz), the module deformation is dominated by the cords. The strips are moving with the cords without entering their own vibration modes. In that range for the symmetric modes, the module vibrates like four cords with lumped masses at the connections with the strips. Above 1 Hz, the strips start vibrating and their own vibration modes are coupled with the ones of the cords. In-planes rotation modes also appear in which each square formed by adjacent strips start ratation with respect to each other. Figure 18 presents some of the modes extracted from the FEM.

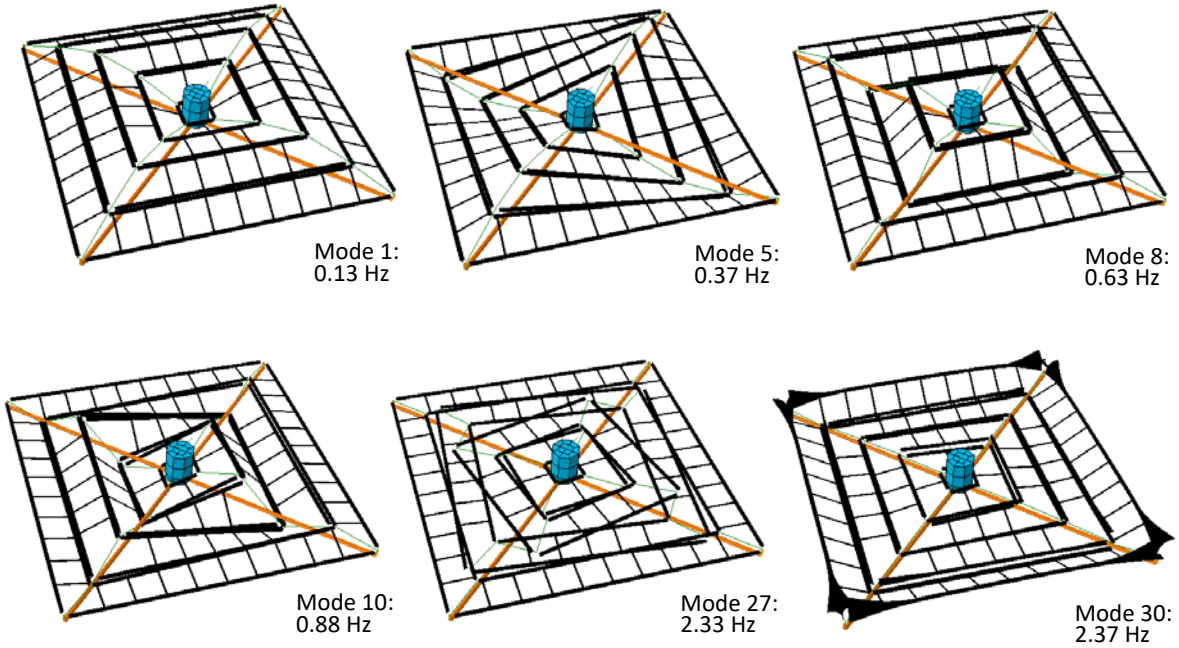

Figure 18. Various module vibration modes. Below approximatively 1 Hz, the cords (in green) are the main drivers for the strips displacement, which follow their attachment points as they move. Above 1 Hz, one can notice that the strips start vibrating, as seen at the outer longerons' end cross-sections in mode 30. One can observe symmetric modes like mode 1, 8 and 30 as well as antisymmetric modes like mode 5 and 10. Several in plan modes also appear (similar to mode 27).

One would like next to understand the influence of the cord prestress on the vibration modes of the structure. The simulation has been repeated for 7 different prestress values: 0.1 N, 1 N, 10 N, 25 N, 50 N, 75 N and 100 N. Figure 19 shows the evolution of the natural frequency of mode 1 to 30 for the considered range of prestress. One can see that the prestress increases the natural frequencies which was expected since the natural frequency of a simple cord increases with the square root of the prestress. It is noticeable that

above approximately 20 N, the influence of the cord prestress becomes less significant and even negligible for some modes (see fifth mode).

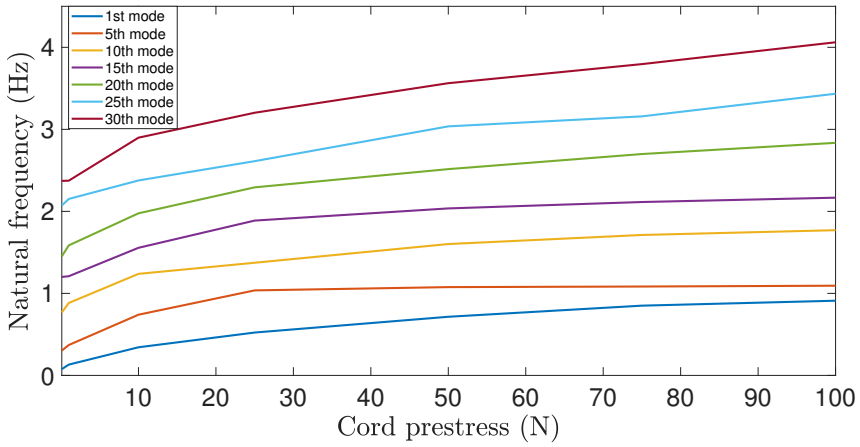

Figure 19. Frequency of selected vibration modes for the 2 m module.

The long term goal is to go from a 2 m prototype to a 60 m structure. As mentioned in the motivation paragraph, the two very distinct length scales at the strip level appears to be a computational challenge as it requires a fine mesh and thus a very consequent number of elements. For the 60 m module this number can go up to 100 million elements. In order to solve this issue the ABAQUS standard substructuring capabilities are used. In this approach, each strip of the quadrant is replaced by a substructure supposed to represent its behavior. The retained degrees of freedom are chosen to be the two end cross-sections of the strip inner and outer longeron. The substructures (sometimes also referred to as superelements) generation step is performed using the so-called Craig-Bampton method. The linear response of each strip is enriched with a linear combination of its 30 first modes or vibration. While this is not needed for the linear perturbation analysis detailed in this paper, it is very important to increase the model fidelity for further dynamics analyses. In order to assess the performance of the substructuring approach we compared the 30 first vibration frequencies obtained using the Craig-Bampton method with the ones extracted from the fully resolved model presented earlier. The relative error in frequency is shown in figure20. Substructuring the model yields some errors, and it is not the same for all the modes. However the absolute and relative error stays constant as the cord prestress increases, which is normal since the connection scheme prevent the strips from being prestressed. The maximum relative error over the 30 first modes is 3.8 % which seems reasonable, and comfort us in the idea that relevant results could be achieve with a larger model.

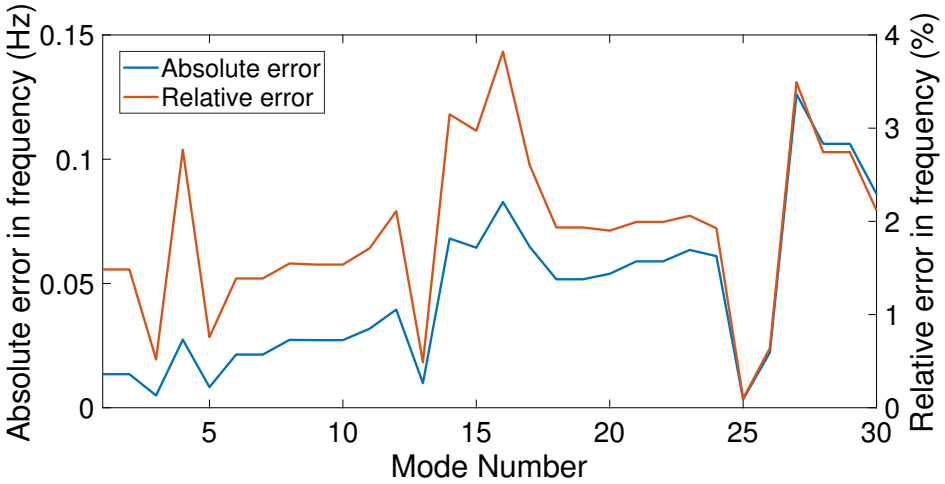

Figure 20. Various vibration modes for the 2 m module.

VI. Conclusion

A new kind of ladder-like coilable space structure has been presented. The main idea consists of linking TRAC longerons with lenticular cross-section battens, which allows the structure to be flattened and coiled. A manufacturing process has been elaborated in order to do quick prototyping of the battens and relies on a novel process using male and female silicone molds enclosed into aluminum caging. The manufacturing of the TRAC longeron uses a variation of a process already established. A reliable connection scheme between the longerons and battens have been designed and testing through the manufacturing of a 54 cm long strip structure. A simple experimental modal test has then been performed on this prototype in order to validate our ability to capture accurately the behavior of this thin shell structure, especially at the batten/longeron connection. From there a full strip finite element model has been generated for various length and modal analyses has been performed. At low frequency the longeron are behaving as two independent beams while at higher frequencies the battens start entering their own vibration modes and the longerons vibration amplitude decreases. The simulation also show that the batten torsional stiffness into the strip stiffness and that the non uniform twist at the batten transition region is non-negligible. The strip model has then been integrated into the spacecraft structure, called the module. A modal analysis has been performed on a 2 m module and showed that below 1 Hz, the vibrations are cord dominated while the strip start entering their own vibration modes above 1 Hz. This analysis has been repeated for various values of cord prestress and shows that above 20 N, the influence of the prestress on the evolution of the module natural frequencies is negligible. Finally if one wants to simulate modules of increasing size, the number of elements needed for the simulation to be accurate becomes rapidly intractable. To cope with this issue, the use of substructure modeling is investigated at the 2 m scale, and shows good performance in terms of relative error in frequency. It paves the way for module simulation of larger size up to the ultimate goal of a 60 m by 60 m structure. For the SPPI application the strip design is not finalized yet and the effort presented in this paper constitutes the first iteration. For instance one needs to refine the design of the 45 deg ends of the strip that are for the moment left unpopulated by battens, and therefore are not optimal in terms of tile density. The influence of the tiles stiffness on the strip structure also has to be investigated. Finally we want to perform dynamic simulations to understand the influence of spacecraft maneuvers and actuators on the module structural response.

Acknowledgments

Financial support from the Northrop Grumman Corporation is gratefully acknowledged.

References

[1]Gdoutos et al (2018). A Lightweight Tile Structure Integrating Photovoltaic Conversion and RF Power Transfer for Space Solar Power Applications. SciTech 2018

[2]Goel, A., Lee, N. and Pellegrino, S. (2017). Trajectory design of formation flying constellation for space-based solar power. IEEE Aerospace Conference, Big Sky, MN

[3]Arya, M., Lee, N. and Pellegrino, S. (2016). Ultralight Structures for Space Solar Power Satellites. SciTech 2016, San Diego, AIAA-2016-1950

[4]Murphey, T.W. and Banik, J., The United States Of America As Represented By The Secretary Of The Air Force, 2011. Triangular rollable and collapsible boom. U.S. Patent 7,895,795.

[5]Hoang, B., White, S., Spence, B. and Kiefer, S., 2016, March. Commercialization of Deployable Space Systems' roll-out solar array (ROSA) technology for Space Systems Loral (SSL) solar arrays. In Aerospace Conference, 2016 IEEE (pp. 1-12). IEEE.

[6]Campbell, D., Barrett, R., Lake, M.S., Adams, L., Abramson, E., Scherbarthn, M.R., Welsh, J.S., Freebury, G., Beidleman, N. and Abbot, J., 2006, March. Development of a novel, passively deployed roll-out solar array. In Aerospace Conference, 2006 IEEE (pp. 9-pp). IEEE.

[7]Leclerc, C., Wilson, L., Bessa, M., and Pellegrino, S. (2017). Characterization of ultra-thin composite triangular rollable and collapsible booms. SciTech 2017, Grapevine (TX), AIAA